Check for updates

ChemCatChem

Research Article
doi.org/10.1002/cctc.202400281

Chemistry Europe
European Chemical Societies Publishing

www.chemcatchem.org

Facile Preparation of Stable Ni^{II}- and Co^{II}-Tetraaminophthalocyanine Electropolymers for Highly Efficient Heterogeneous Carbon Dioxide Reduction

Jirapong Luangchaiyaporn,[a] Permsak Chairat,[a] Rapheepraew Sodkhomkhum,[a] Niyazi Serdar Sariciftci,[b] and Patchanita Thamyongkit*[a]

This study focused on preparation of stable polymer films of Ni^{II}- and Co^{II}-tetraaminophthalocyanines, **p-NiTAPc** and **p-CoTAPc**, respectively, for highly efficient heterogeneous electrochemical carbon dioxide (CO_2) reduction in a flow electrolysis cell. Major development represented in this work was fabrication of **p-NiTAPc** and **p-CoTAPc** films via electropolymerization of their corresponding monomers on carbon-based substrates without using binder or conducting additive materials to obtain efficient gas diffusion electrodes (GDEs) for scalable, productive and selective CO_2-to-CO conversion. The target polymers were characterized by UV-visible spectrophotometry, attenuated total reflection-Fourier transform infrared spectroscopy, scanning electron microscopy, energy dispersive X-ray spectroscopy and cyclic voltammetry. According to controlled potential electrolysis and gas chromatography, **p-NiTAPc**-catalyzed CO_2 reduction at −0.99 V *vs.* reversible hydrogen electrode (RHE) gave 953 mL of CO in a period of 16 hours with current density and Faradaic efficiency (FE) of 109 ± 1 mA·cm^{-2} and 99 ± 2%, respectively. A **p-CoTAPc**-modified GDE exhibited superior catalytic performance to the case of **p-NiTAPc** in terms of catalyst stability and CO productivity by performing the continuous CO_2 reduction at the potential of −1.10 V *vs.* RHE for up to 41 hours and affording almost 3 times higher amount of CO with the current density of 161 ± 5 mA·cm^{-2} and 95 ± 2% FE.

Introduction

Increase in atmospheric carbon dioxide (CO_2) levels since the industrial revolution has resulted in significant climate change and ocean acidification.[1] To mitigate these issues, various CO_2 reduction methods, including chemical,[2] photochemical,[3] electrochemical,[3a,4] and biological ones.[5] Among these approaches, electrochemical CO_2 reduction reaction (CO_2RR) is known to be practical as it can be performed in aqueous solutions at ambient condition using renewable energy sources,[4,6] leading to possible formation of significant amounts of various products, such as formic acid, carbon monoxide (CO), alcohols, methane, and ethylene.[2] However, efficient catalysts, especially heterogeneous kinds, are required to achieve selectivity towards the reduction of the inert CO_2 molecules over competing hydrogen (H_2) evolution reaction (HER) in aqueous electrolytes, and high productivity of desired product(s).[4a,7] State-of-the-art heterogeneous catalysts containing metals (Au, Ag, and Cu),[8] metal alloys (Cu–Au, Cu–Sn, Cu–Pd, etc.),[9] metal oxides (Cu/SnOx, PtO_2, RhO_2),[10] transition-metal chalcogenides (MoS_2, $MoSe_2$, and WSe_2)[11] and transition-metal complexes (Co-, Fe-, Ni-, Cu- based N_4-ligands complexes)[12] have been reported to exhibit high electrocatalytic performance for the CO_2RR in the aqueous electrolytes. Among these catalysts, Ni^{II}- and Co^{II}-phthalocyanines (**NiPc** and **CoPc**, respectively) and their derivatives are effective catalysts for production of CO from the CO_2RR due to their high stability and tunability of their electrochemical properties by several possible structural modification to achieve high Faradaic efficiency (FE).[13] CO is known to be an attractive product due to its low energy consumption, ease of separation from electrolyzers, and potential use as a feedstock for industrial chemical production.[14] However, aggregation of the Pc macrocycles on the electrode surface is a common issue that leads to high electrical resistance of the calatyst films and, consequently, poor catalytic performance.[13,15] Some carbon-based semiconductive materials, such as carbon nanotubes (CNTs), and binders are often used to form blended film with Pc to improve film conductivity and/or morphology. However, additional steps and more complicated preparation procedures may lead to low repeatability in the film formation process, and can be more expensive and time consuming. An alternative method for alleviating the Pc aggregation is electrochemical polymerization of Pc monomers containing electropolymerizable peripheral substituents.[16] According to our previous report, electropolymerization of a bithienyl-functionalized Pc monomer could give the corresponding polymer having desirable film morphologies

[a] *Dr. J. Luangchaiyaporn, P. Chairat, R. Sodkhomkhum, Prof. Dr. P. Thamyongkit*
Department of Chemistry
Faculty of Science, Chulalongkorn University
Bangkok 10330, Thailand
E-mail: patchanita.v@chula.ac.th

[b] *Prof. Mag. Dr. DDr. N. S. Sariciftci*
Linz Institute for Organic Solar Cells (LIOS), Institute of Physical Chemistry
Johannes Kepler University Linz
4040 Linz, Austria

Supporting information for this article is available on the WWW under https://doi.org/10.1002/cctc.202400281

© 2024 Wiley-VCH GmbH

and exhibiting high electrocatalytic activity in the CO_2RR without using any binders and CNTs.[16a]

In this research, we presented preparation of polymer films of Ni^{II}- and Co^{II}-4,9,16,23-tetraaminophthalocyanine (**NiTAPc** and **CoTAPc**, respectively, Figure 1) and investigation on their catalytic performance for the electrochemical CO_2RR. We hypothesized that the presence of amino groups in **NiTAPc** and **CoTAPc** monomers would facilitate oxidative electropolymerization, resulting in the efficient direct formation of the target polymer films, namely **p-NiTAPc** and **p-CoTAPc**, onto the electrode without the need for the binder. Additionally, the remaining amino units on the polymers may contribute to CO_2 capture during the CO_2RR, as reported in several CO_2 capture studies.[17] The electropolymerization of amino-containing metallated phalocyanines (MPcs) and characterizarion of the resulting MPc-based polymer films were previously studied, but the use of those MPc films for the CO_2RR has not been reported before.[18] According to previous electrochemical CO_2 conversion in electrolyzers with H-type and flow cell configurations,[19] this work further developed the flow cell for the CO_2RR by using **p-NiTAPc-** and **p-CoTAPc**-coated gas diffusion electrodes (GDEs) that allowed increase in CO_2 concentration on catalyst surface and enhanced production rate of the CO_2RR products at high current densities (above 100 $mA \cdot cm^{-2}$). Further cell improvement to achieve long operation time with high productivity and selectivity at working reduction potential by introducing a hydrophobic polytetrafluoroethylene (PTFE)[20] coating layer on the GDE was also explained herein.

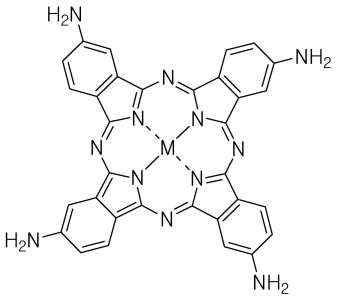

NiTAPc; M = Ni
CoTAPc; M = Co

Figure 1. A general structure of target monomers.

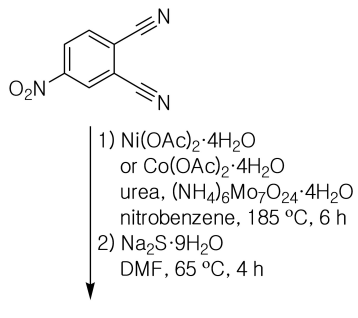

NiTAPc (56%); M = Ni
CoTAPc (50%); M = Co

Scheme 1. Synthesis of **NiTAPc** and **CoTAPc** monomers.

Results and Discussion

1. Polymer Synthesis and Film Preparation

Synthesis of **CoTAPc** and **NiTAPc** monomers was performed by self-condensation of 4-nitrophthalonitrile in the presence of corresponding metal acetate, urea, ammonium molybdate in nitrobenzene at 185 °C for 6 hours according to a previously reported method[21] (Scheme 1). Subsequently, the resulting metal-chelated tetranitrophthalocyanine products was directly reduced by sodium sulfide in dimethylformamide (DMF) at 65 °C for 4 hours to give the desirable tetraamino products **NiTAPc** and **CoTAPc** in 56% and 50% yield, respectively. Formation of **NiTAPc** and **CoTAPc** was confirmed by high resolution matrix-assisted laser desorption/ionization time-of-flight mass spectrometry (HR-MALDI-TOF MS) at molecular ion peaks at *m/z* 630.1291 and 631.1291, respectively.

The electropolymerization of **NiTAPc** and **CoTAPc** was performed on pre-treated indium tin oxide-coated glasses (ITO-glass) and microporous layers (MPLs) of the commercial carbon fiber papers (CFPs) using cyclic voltammetry (CV) in a three-electrode one-compartment cell to obtain the **p-NiTAPc** and **p-CoTAPc** films, respectively. The cell consisted of the ITO-glass or MPL-CFP substrate as a working electrode (WE), a AgCl-coated Ag wire (Ag/AgCl) as a quasi-reference electrode (QRE), and a Pt wire as a counter electrode (CE). A supporting electrolyte solution used was a 0.1 M tetrabutylammonium hexafluorophosphate ($TBAPF_6$) in dimethyl acetamide (DMAC) and contained 0.5 mM **NiTAPc** or **CoTAPc**. The resulting films of **p-NiTAPc** and **p-CoTAPc** on the ITO-glasses (**p-NiTAPc**/ITO-glass and **p-CoTAPc**/ITO-glass, respectively) were subjected to film characterization, while those on the MPL-CFP substrates (**p-NiTAPc**/MPL-CFP and **p-CoTAPc**/MPL-CFP, respectively) were investigated for their electrochemical behavior by the CV technique and used as the GDE in a flow electrochemical cell for catalytic performance studies. Due to complicated morphology of the polymer-coated MPL-CFP, the current densities reported throughout this work were referred to geometric surface of the electrode, and electrochemically active coverage of each polymer film was determined by total charge integration in the CV experiments and used to calculate turnover frequency (TOF). This approach has been used by several works relating to Pc-coated/blended electrocatalysts for the CO_2RR.[19d,29b,30]

Figure 2 presents cyclic voltammograms of the electropolymerization of **NiTAPc** and **CoTAPc** in a potential range of −0.33 V to 1.27 V *vs.* normal hydrogen electrode (NHE) at a scan rate of 50 $mV \cdot s^{-1}$. The potential was cycled in a positive potential range to oxidize the amino groups on the macrocycles to generate radical cation, leading to the polymerization, and then in a negative region to stabilize the charge of the resulting polymers and ions in the electrolyte. During the first oxidative scanning cycle, the electropolymerization of **NiTAPc** exhibited two oxidative peaks at around 0.75 V and 1.06 V *vs.* NHE for both substrates, which may be due to oxidation of primary amino groups and a Pc ligand in the molecule, respectively.[16b,22] A Ni^{2+}/Ni^{3+} oxidative process was not

© 2024 Wiley-VCH GmbH

18673899, 0, Downloaded from https://chemistry-europe.onlinelibrary.wiley.com/doi/10.1002/cctc.202400281 by Faculty Of Medicine, Library Chulalongkorn University, Wiley Online Library on [09/06/2024]. See the Terms and Conditions (https://onlinelibrary.wiley.com/terms-and-conditions) on Wiley Online Library for rules of use; OA articles are governed by the applicable Creative Commons License

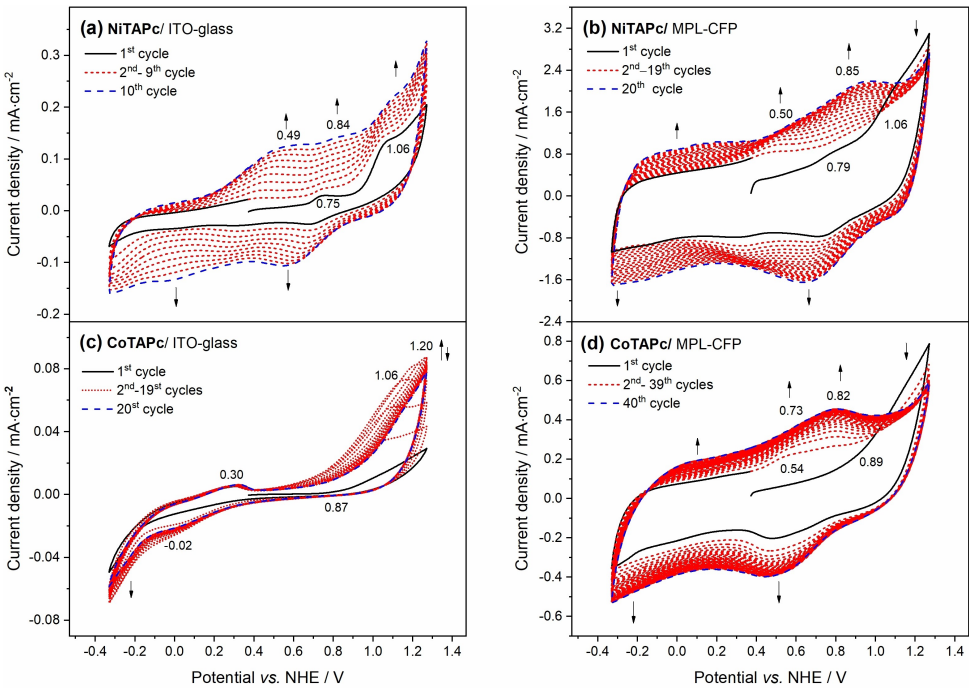

Figure 2. The cyclic voltammograms of the electrochemical polymerization of **NiTAPc** on (a) the ITO-glass and (b) the MPL-CFP, and of **CoTAPc** on (c) the ITO-glass and (d) the MPL-CFP. Black solid, red dotted and blue dashed lines represent the first, the intermediate and the last scanning cycles, respectively.

observed in this potential window. As the number of scanning cycles increased, new oxidation peaks and an increase in the current density were observed at around 0.49 V, 0.84 V, and 1.06 V *vs.* NHE on both ITO-glass and MPL-CFP substrates. The cyclic voltammogram of **CoTAPc** at the first cycle showed the enhanced current density at a potential onset of around 0.87 V *vs.* NHE on the ITO-glass and 0.89 V *vs.* NHE on the MPL-CFP, likely due to the oxidation of the primary amino groups.[22a,c–e,23] While a Co^{2+}/Co^{3+} oxidation peak could be observed at 1.06 V *vs.* NHE during the polymerization on the ITO-glass, this peak might be overlapped with a broad signal of the amino group oxidation in the case of the polymer formation on the MPL-CFP. According the previously published report, a reduction peak at −0.02 V *vs.* NHE observed on the ITO-glass might be due to a Co^{2+}/Co^{1+} reduction process.[22c–e,23] Upon increasing the number of the scanning cycles, shift of potential onsets from 0.57 V to 1.20 V *vs.* NHE was observed for the electropolymerization on the ITO-glass, while new oxidative peaks at 0.73 V and 0.82 V *vs.* NHE became pronounced when the MPL-CFP was used. The increase in the current density and the formation of new oxidative peaks observed for both monomers could indicate the formation of new electroactive species on the electrode surface, possibly the oxidation of the monomer to form oligomer or polymer species via radical cation formation of the amino groups.[16b,22a,b,d,e,23] Due to low solubility of **CoTAPc**, a higher number of the scanning cycles, compared with the case of **NiTAPc**, was required for its electropolymerization on both substrates.

The formation of the polymer films, **p-NiTAPc** and **p-CoTAPc**, on the electrode surfaces was confirmed by UV-visible (UV-vis) spectrophotometry, attenuated total reflectance-Fourier transform infrared (ATR-FTIR) spectroscopy, scanning electron microscopy (SEM) and energy-dispersive X-ray spectroscopy (EDS). In Figure 3, UV-vis spectrum of the **p-NiTAPc** film on the ITO-glass (**p-NiTAPc**/ITO-glass) showed broad B-bands at 297 nm and 429 nm, and Q-bands at 647 nm and 732 nm. These peak patterns were consistent with absorption character-

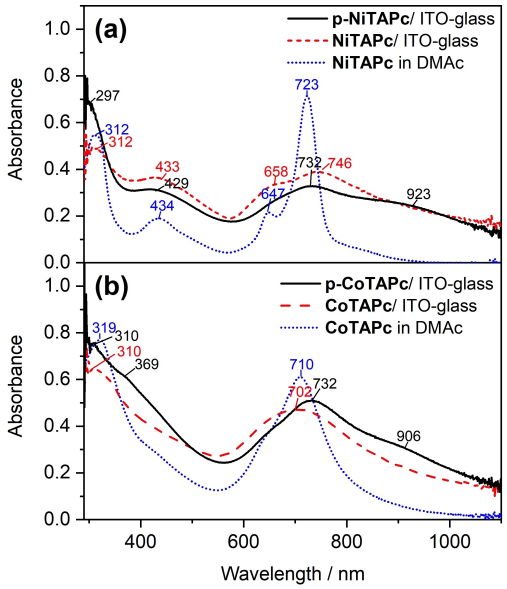

Figure 3. The UV-vis spectra of the polymer films on the ITO-glass (black solid line), compared with those of the monomer drop-casted films on the ITO-glass (red dashed line) and the monomer solution in DMAc (blue dotted line) for the case of (a) **p-NiTAPc** and **NiTAPc**, and (b) **p-CoTAPc** and **CoTAPc**.

© 2024 Wiley-VCH GmbH

18673899, 0, Downloaded from https://chemistry-europe.onlinelibrary.wiley.com/doi/10.1002/cctc.202400281 by Faculty Of Medicine, Library Chulalongkorn University, Wiley Online Library on [09/06/2024]. See the Terms and Conditions (https://onlinelibrary.wiley.com/terms-and-conditions) on Wiley Online Library for rules of use; OA articles are governed by the applicable Creative Commons License

istics of a **NiTAPc** drop-casted film on the ITO-glass (**NiTAPc**/ITO-glass) and a **NiTAPc** solution in DMAc. Similarly, an absorption spectrum of the **p-CoTAPc** film on the ITO-glass (**p-CoTAPc**/ITO-glass) exhibited broad absorption features of the B-bands at around 310 nm and 369 nm, and the Q-band at 732 nm, corresponding to those of a **CoTAPc** drop-casted film on the ITO-glass (**CoTAPc**/ITO-glass) and a **CoTAPc** solution in DMAc. The broader feature and slight red shift observed for the polymer and monomer films on the ITO-glass, compared with their monomer solutions, were likely due to H-aggregation of the Pc macrocycles.[24] Furthermore, additional peaks observed at around 923 nm for **p-NiTAPc** and 906 nm for **p-CoTAPc** were possibly indicative of the formation of delocalization species in the extended polymer network.[25]

ATR-FTIR spectra of **p-NiTAPc**, **p-CoTAPc** and their corresponding monomers were examined in a range of 650 cm^{-1} to 1800 cm^{-1} and around 3300 cm^{-1}. Characteristic vibrational peaks at 754 cm^{-1}, 827 cm^{-1}, 1101 cm^{-1}, 1313 cm^{-1}, 1352 cm^{-1} and 1413 cm^{-1}, indicating the presence of a π-conjugate system in a macrocycle skeleton of phthalocyanine,[26] were detected in all samples (Figure 4). Appearance of a new peak at 1504 cm^{-1} and the positive shift of the peak from 1604 cm^{-1} observed for the monomers to 1614 cm^{-1} for the polymer films possibly came from transformation of NH_2 scissoring vibration of the monomers to the benzenoid ring stretching in the polymers.[26]

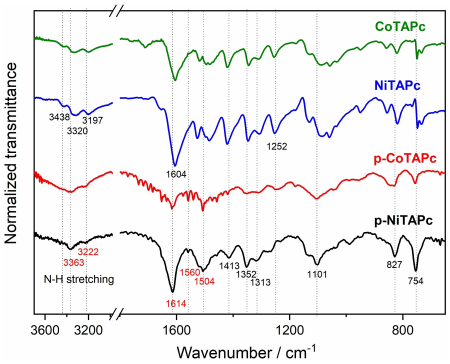

Figure 4. The ATR-FTIR spectra of the **p-NiTAPc** (black line) and **p-CoTAPc** (red line) films, and their monomer **NiTAPc** (blue line) and **CoTAPc** (green line) powder samples.

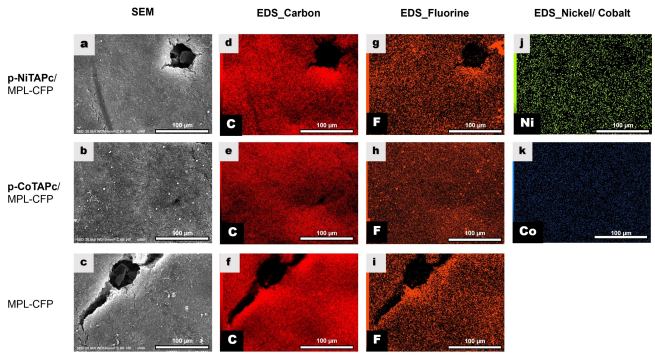

Figure 5. The SEM images of (a) **p-NiTAPc**/MPL-CFP and (b) **p-CoTAPc**/MPL-CFP, in comparison with (c) MPL-CFP, and EDS mapping of (d-f) carbon, (g-i) fluorine, (j) nickel and (k) cobalt atoms in each sample.

Additionally, new N–H stretching vibration bands at 3363 cm^{-1} and 3222 cm^{-1} appeared in the spectra of the polymers, compared with those at 3238 cm^{-1}, 3320 cm^{-1} and 3197 cm^{-1} observed for the monomers, affirming the formation of secondary amine units in both polymer networks.[27] This observation was consistent with a previously proposed oxidative coupling mechanism for the electropolymerization of the amino-containing metallated phthalocyanines, where the formation of the secondary amine linkges was involved.[18]

SEM and EDS were employed to investigate attachment and distribution of the polymer films on the MPL-CFP. As shown in Figure 5, compared with SEM images, the EDS analysis of the polymer films and the pristine MPL-CFP substrates revealed the presence of carbon and fluorine atoms, originating from CP and PTFE, respectively. Only EDS mapping of the polymers films on the MPL-CFP exhibited nickel or cobalt atoms evenly scattered on the substrates, suggesting good coverage of **p-NiTAPc** and **p-CoTAPc**, respectively, on the MPL-CFP surface.

2. Electrocatalytic Performance

2.1. Continuous Flow Electrolysis at Different Reduction Potential

The electrocatalytic activity of **p-NiTAPc** and **p-CoTAPc** was studied by the CV and controlled potential electrolysis (CPE) using the flow electrochemical cell, a setup of which is depicted in Figure 6. The cell consisted of a gas flow channel located on a PTFE plate, which was placed adjacent to a PTFE-coated CFP (PTFE-CFP) side of the GDE. On the opposite side of the GDE, the **p-NiTAPc**/MPL-CFP or **p-CoTAPc**/MPL-CFP, used as the WE, was exposed to a flowing catholyte solution in a catholyte chamber having a Ag/AgCl (3 M KCl) reference electrode (RE). An anolyte chamber containing the Pt wire as the CE was separated from the catholyte one by an anion exchange membrane (AEM). An aqueous solution of 1 M $KHCO_3$ was flown into both chambers at a flow rate of 15 mL·min^{-1}. Both GDE and CE were attached by Ti plates as current collectors. When the cell was tightly assembled with nuts, silicone rubber sheets served as sealing gaskets to prevent leakage of CO_2 and the electrolyte solution. CO_2 was flown in the flow channel at the rate of 10 mL·min^{-1}.

The cyclic voltammograms of **p-NiTAPc** in a 1 M $KHCO_3$ solution in Figure 7a exhibited reduction peaks at 0.35 V and −0.27 V *vs.* reversible hydrogen electrode (RHE), attributed to a reduction of the macrocyclic ligand and either partial reduction of Ni^{I}/Ni^{II} or the second reduction of the macrocyclic ligand, respectively.[29]

Under the same measurement condition, the cyclic voltammograms of **p-CoTAPc** exhibited typical reduction peaks at 0.14 V *vs.* RHE, which was associated with Co^{II}/Co^{I} transition (Figure 7b and inset).[16a,30] Enhancement of the current density was observed at onset potential of −0.38 V and −0.33 V *vs.* RHE for **p-NiTAPc** and **p-CoTAPc**, respectively.

The CPE and product analysis by GC were carried out to monitor the CO_2RR product(s) and the catalytic performance of

© 2024 Wiley-VCH GmbH

18673899, 0, Downloaded from https://chemistry-europe.onlinelibrary.wiley.com/doi/10.1002/cctc.202400281 by Faculty Of Medicine, Library Chulalongkorn University, Wiley Online Library on [09/06/2024]. See the Terms and Conditions (https://onlinelibrary.wiley.com/terms-and-conditions) on Wiley Online Library for rules of use; OA articles are governed by the applicable Creative Commons License

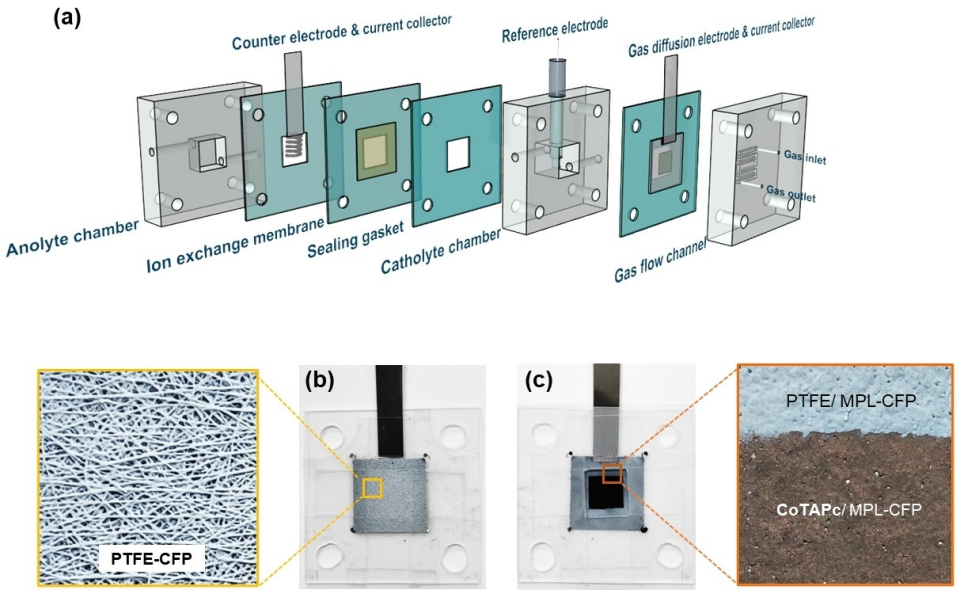

Figure 6. (a) A schematic setup of flow cell components, and images of (b) the PTFE-CFP and (c) the **p-CoTAPc**/MPL-CFP with insets showing their microscopic perspectives.

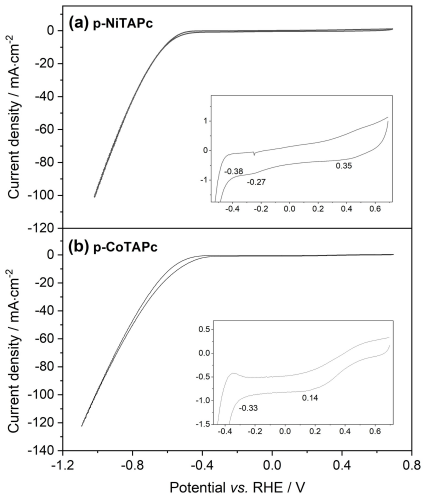

Figure 7. The cyclic voltammograms of (a) **p-NiTAPc**/MPL-CFP and (b) **p-CoTAPc**/MPL-CFP in the CO_2 (10 mL·min^{-1}) flow cell using the 1 M $KHCO_3$ electrolyte solution (15 mL·min^{-1}) at the scan rate of 50 mV·s^{-1}.

the **p-NiTAPc**/MPL-CFP and **p-CoTAPc**/MPL-CFP at various potentials. At the beginning of each experiment, the potential was hold at −0.84 V *vs.* RHE for 1 hour equilibration time to obtain stable current signal and then a series of the potential of −0.84 V, −0.91 V, −0.99 V, −1.05 V and −1.16 V *vs.* RHE for **p-NiTAPc**, or −0.84 V, −0.93 V, −1.00 V, −1.05 V, −1.10 V, −1.14 V and −1.22 V *vs.* RHE for **p-CoTAPc** was consecutively applied for 4 hours at each step. The productivity of the reduction product formation was determined after the equilibration time. As shown in Figure 8a, chronoamperometric responses of the CO_2RR under catalysis of the **p-NiTAPc**/MPL-CFP represents steady current density throughout the period of 4 hours at each potential step, starting from 57 ± 0.8 mA·cm^{-2} at −0.84 V *vs.* RHE to 96 ± 1.1 mA·cm^{-2} at −0.99 V *vs.* RHE. The GC analysis indicated the comparable FE for CO formation (FE_{CO}) of approximately 95%, without significant detection of H_2 (Figure 8b). Upon further potential increment to −1.05 V *vs.* RHE, the current density rose to 118 ± 1.7 mA·cm^{-2} for the first 2 hours and then began to decline to 112 ± 2.7 mA·cm^{-2} with 96 ± 3% FE_{CO}. However, when the reduction potential was increased to −1.16 V *vs.* RHE, the current density initially rose to 132 mA·cm^{-2}, but then rapidly decreased to 103 ± 0.8 mA·cm^{-2}. The drop in the current density, possibly caused by high charge accumulation in the GDE during the CO_2RR, leading to hydrophobicity loss of the electrode (or electrode wetting), rapid formation of H_2 gas and/or carbonate salts, and the possible breakdown of the catalyst film.[31] These possible scenarios could contribute to the deterioration of the electrode structure and the PTFE coating, as evidenced by the leakage of the electrolyte solution (flooding) from the gas outlet of the CO_2 flow channel and the small cracking area of the PTFE-CFP observed after completion of the electrolysis (**Figures S7** and **S8**). The flooding might block CO_2 from getting to the catalyst side, resulting in more H_2 production and the lower selectivity of the CO formation. As a result, the FE_{CO} was decreased to 66 ± 16% with the gradual occurrence of H_2 to 21 ± 13% avaerage FE in the last 4-hour interval.

Quantitative determination of the product formation expressed in Figure 8c indicated accumulation of products observed in the 4-hour intervals to be 98 mL, 129 mL, 169 mL, 207 mL, and 148 mL at −0.84 V, −0.91 V, −0.99 V, −1.05 V and −1.16 V *vs.* RHE, respectively, with the H_2 production of 42 mL at −1.16 V *vs.* RHE. Due to the stable current density level of CO_2 to CO conversion with high %FE, selectivity and yield, the applied potential of −0.99 V *vs.* RHE was selected for stability study discussed in the next section.

In the case of the **p-CoTAPc**-catalyzed CO_2RR, when the applied potential was raised from −0.84 V to −1.05 V *vs.* RHE,

© 2024 Wiley-VCH GmbH

18673899, 0, Downloaded from https://chemistry-europe.onlinelibrary.wiley.com/doi/10.1002/cctc.202400281 by Faculty Of Medicine, Library Chulalongkorn University, Wiley Online Library on [09/06/2024]. See the Terms and Conditions (https://onlinelibrary.wiley.com/terms-and-conditions) on Wiley Online Library for rules of use; OA articles are governed by the applicable Creative Commons License

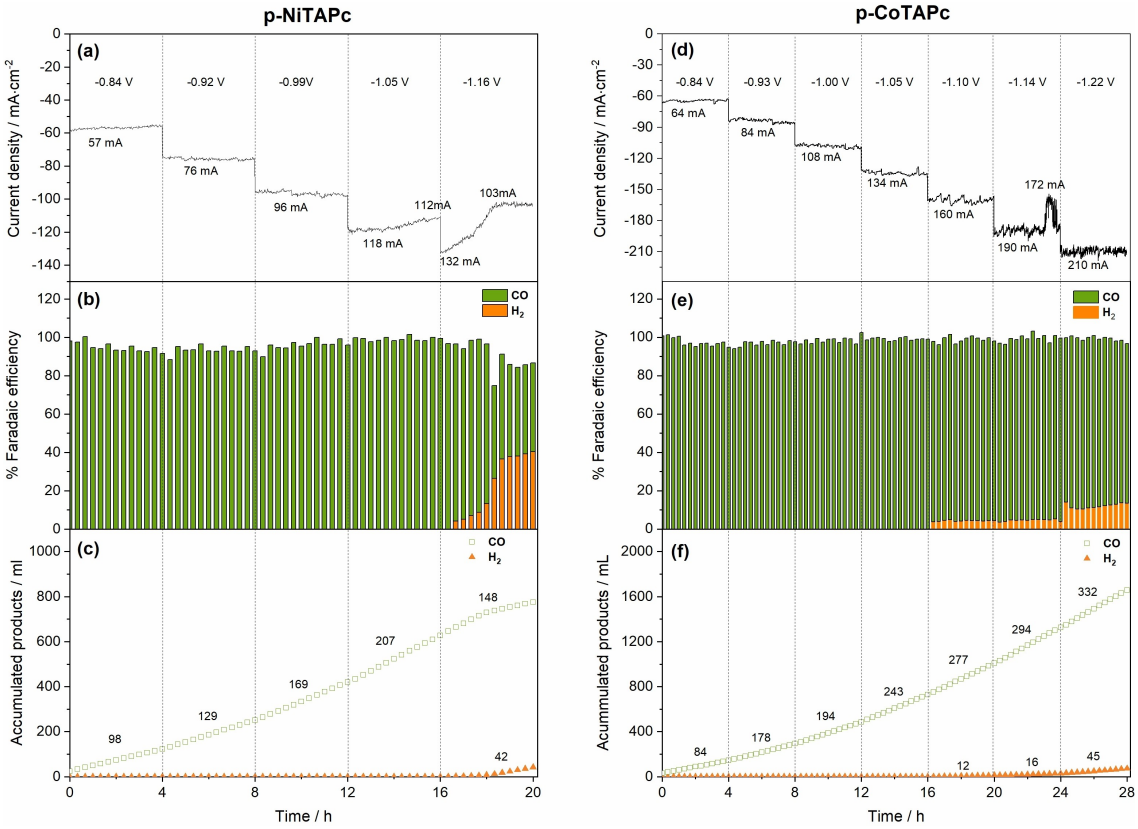

Figure 8. (a) Chronoamperometric responses of the **p-NiTAPc**- and **p-CoTAPc**-catalyzed CO_2RR at various potentials, (b) the % FE for the CO and H_2 formation and (c) the accumulated amounts of products at each 4-hour interval. The CPE was performed in the flow cell using the flow rates of CO_2 and the 1 M $KHCO_3$ solution of 10 and 15 mL·min^{-1}, respectively, at the scan rate of 50 mV·s^{-1}.

the current density was found to be stable in each 4-hour period and increased from 64 ± 0.5 mA·cm^{-2} to 134 ± 1.8 mA·cm^{-2}, respectively (Figure 8d). In this potential range, CO was found as the only product with 98 ± 2% FE and the accumulated amounts of CO were 84 mL, 178 mL, 194 mL, 243 mL and 277 mL at −0.84 V, −0.93 V, −1.00 V, −1.05 V *vs.* RHE, respectively (Figures 8e and **8f**). When the potential reached −1.10 V *vs.* RHE, the current density was further increased and remained steady at 160 ± 2.6 mA·cm^{-2} with observation of the CO and H_2 formation at 95 ± 1.4% and 4 ± 0.3% FE, and the product accumulation of 277 mL and 12 mL, respectively. At the potential of −1.14 V *vs.* RHE, the current density was increased and steady at 190 ± 3.2 mA·cm^{-2} for 3 hours before dropping to 172 ± 12 mA·cm^{-2}. The higher productivity of CO was detected with 95 ± 1.7% FE_{CO} and 294 mL accumulated CO amount, while the H_2 production was found to be still small, *i.e.* with 5 ± 0.5% FE_{H2} and 16 mL accumulated H_2 amount. The drop in the current density resulted from the electrode wetting and flooding as observed in the case of **p-NiTAPc**. However, upon the potential elevation to −1.22 V *vs.* RHE, the current density was found to be stabilized at 210 ± 2.5 mA·cm^{-2} with slightly fuzzy pattern possibly due to the rapid formation of gas bubbles as observed from the outlet of the catholyte chamber. At this potential, the product formation was found to be less selective by showing 87 ± 2.2% FE_{CO} and 12 ± 1.3% FE_{H2} with increase in CO and H_2 accumulative amounts to 332 mL and 45 mL, respectively.

According to the above observation, **p-CoTAPc** presented superior catalytic performance in the CO_2RR by showing the higher current density, %FE_{CO} and the product amounts at all potential, and seemed to be resistant to higher potential level, compared to **p-NiTAPc**. This result was consistent with a previous study by Q. Chang et al. on a role of transition metal centers in modifying binding energies of key intermediates involved in the CO_2RR and HER. This study showed that **CoPc** exhibited optimal binding strength of the reaction intermediate on the active Co centers, compared to other MPcs, including **NiPc**.[13b] However, to avoid the leakage of the electrolyte solution and the degradation of the polymer film, the selected potential for the stability test of **p-CoTAPc** was −1.10 V *vs.* RHE.

2.2. Stability Study of the Polymer Films under Operating Condition

The stability of the polymer catalysts was evaluated using the CPE at the applied potentials of −0.99 V and −1.10 V *vs.* RHE for **p-NiTAPc** and **p-CoTAPc**, respectively. The results in Figure 9 showed that the current density of the **p-NiTAPc**-catalyzed CO_2RR was quite stable at 109 ± 1 mA·cm^{-2} for the first 15.8 hours (Figure 9a) with the %FE_{CO} of 99 ± 2% (Figure 9b).

© 2024 Wiley-VCH GmbH

18673899, 0, Downloaded from https://chemistry-europe.onlinelibrary.wiley.com/doi/10.1002/cctc.202400281 by Faculty Of Medicine, Library Chulalongkorn University, Wiley Online Library on [09/06/2024]. See the Terms and Conditions (https://onlinelibrary.wiley.com/terms-and-conditions) on Wiley Online Library for rules of use; OA articles are governed by the applicable Creative Commons License

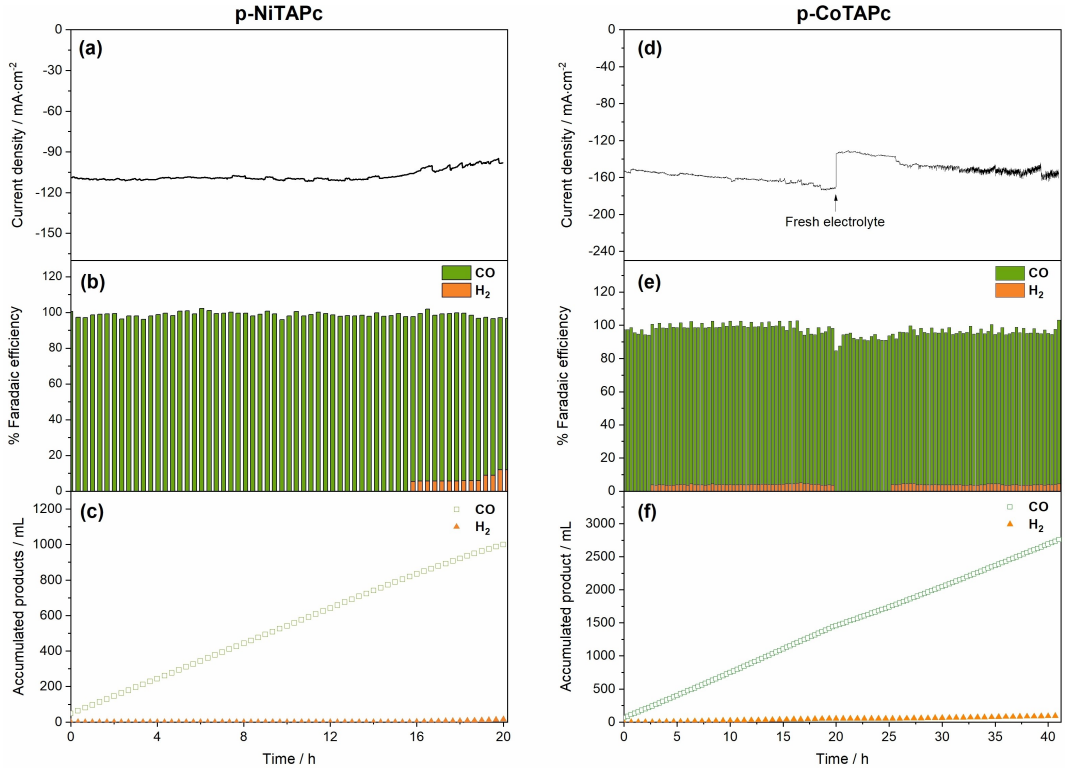

Figure 9. (a) Chronoamperometric responses, (b) the % FE values for the CO_2 and H_2 production, and (c) amounts of CO_2 and H_2 during the 20-hour CO_2RR catalyzed by **p-NiTAPc** and and **p-CoTAPc**- at −0.99 V and −1.10 V *vs.* RHE, respectively. The experiments were performed in the flow cell using the flow rates of CO_2 and the 1 M $KHCO_3$ electrolyte solution of 10 mL·min^{-1} and 15 mL·min^{-1}, respectively.

After that until the reaction was stopped at 20 hours, the current density and the %FE_{CO} were found to decrease to 100 ± 3 mA·cm^{-2} and 91 ± 3%, respectively, with the formation of H_2 of up to 7 ± 2.3% FE. This 20-hour CO_2RR gave total CO and H_2 amounts of 953 mL and 15 mL, respectively (Figure 9c). According to the total charge integration in the CV experiments, the electrochemically active coverage of **p-NiTAPc** on the MPL-CFP substrate was determined to be 1.8×10^{-8} mol·cm^{-2}. Therefore, the average TOF of the CO production in the period of 15.8 hours, when the CPE showed the stable current density, was calculated to be 31 ± 0.34 s^{-1}.

As for the CO_2RR under catalysis of **p-CoTAPc** at the selected potential of −1.10 V *vs.* RHE, showed the current density of approximately 161 ± 5 mA·cm^{-2} for the first 20 hours with 95 ± 2% FE_{CO} and 4 ± 0.3% FE_{H2} (Figures 9d and **9e**), and 1,392 mL CO 52 mL H_2 accumulative amounts (Figure 9f). The slow increase in the current density observed in this 20-hour interval could be attributed to formation of ionic species in this efficient CO_2RR process, resulting in pH shift, and increase in ionic strength and conductivity of the $KHCO_3$ buffer system. Since the CO_2RR was still productive in terms of FE and the product quantity, further investigation was pursued for additional 20 hours by changing the electrolyte solution and continuously monitoring the current density. The results showed that the current immediately reduced to 132 mA·cm^{-2} and stayed at a steady value of approximately 160 mA·cm^{-2} afterwards. The FE_{CO} and FE_{H2} were found to be 92 ± 2% and 2 ± 2%, respectively, and additional 2,691 mL CO and 92 mL H_2 were obtained in the second 20-hour interval. The electrochemically active coverage of **p-CoTAPc** on the MPL-CFP substrate was investigated and found to be about 3 times lower than that of **p-NiTAPc**, *i.e.* 5.6×10^{-9} mol·cm^{-2} *vs.* 1.8×10^{-8} mol·cm^{-2}, resulting in the significantly higher TOF of the CO production for the first 20 hours, *i.e.* 140 ± 4.0 s^{-1}, compared to that of **p-NiTAPc**/MPL-CFP.

These observations suggested that although the CO_2RR using **p-CoTAPc**/MPL-CFP as the GDE produced a trace amount of H_2, the **p-CoTAPc**/MPL-CFP showed superior catalytic performance to the previously reported **Ni-** and **CoPc**-based electrodes in terms of the stability under working condition, TOF and CO_2-to-CO productivity (**Table S1**).

Conclusions

In this study, we report the preparation the **p-CoTAPc** and **p-NiTAPc** electropolymers on the MPL-CFP substrates to serve as the GDEs in the CO_2RR flow cell. The successful formation of the desired polymers was confirmed through characterization using the UV-vis spectrophotometry, the ATR-FTIR spectroscopy, the SEM and the EDS. By means of the CV and the CPE, the optimum working potential for the CO_2RR under the catalysis of each polymer in the flow cell using the flow rates of CO_2 and the aqueous 1 M $KHCO_3$ electrolyte solution of 10 mL·min^{-1} and 15 mL·min^{-1}, respectively, was determined to be −0.99 V and −1.10 V *vs.* RHE for **p-NiTAPc** and **p-CoTAPc**, respectively.

© 2024 Wiley-VCH GmbH

18673899, 0, Downloaded from https://chemistry-europe.onlinelibrary.wiley.com/doi/10.1002/cctc.202400281 by Faculty Of Medicine, Library Chulalongkorn University, Wiley Online Library on [09/06/2024]. See the Terms and Conditions (https://onlinelibrary.wiley.com/terms-and-conditions) on Wiley Online Library for rules of use; OA articles are governed by the applicable Creative Commons License

18673899, 0, Downloaded from https://chemistry-europe.onlinelibrary.wiley.com/doi/10.1002/cctc.202400281 by Faculty Of Medicine, Library Chulalongkorn University, Wiley Online Library on [09/06/2024]. See the Terms and Conditions (https://onlinelibrary.wiley.com/terms-and-conditions) on Wiley Online Library for rules of use; OA articles are governed by the applicable Creative Commons License

At the selected potentials, the **p-NiTAPc** and **p-CoTAPc** films were found to be stable for at least 15.8 and 20 hours, and CO was obtained from the CO_2RR as the main product with 99% and 91% FE, and the TOF of $31 \pm 0.34\ s^{-1}$ and $140 \pm 4.0\ s^{-1}$, respectively. The CO_2RR for extended reduction time of up to 41 hours was proved possible for the case of **p-CoTAPc** when the electrolyte solution was refreshed. These results showed the excellent catalytic performance of **p-NiTAPc** and **p-CoTAPc** in terms of the CO productivity, selectivity, TOF and film stability. This study suggested the promising approach to achieve the highly efficient heterogeneous CO_2RR under the catalysis of the stable electropolymers prepared via a simple binder-/additive-free electrochemical film formation technique that is practical for further use in the large-scale CO_2RR.

Experimental Section

Materials and Methods

All chemicals were obtained from commercial vendors and used as received, unless stated otherwise. ^{1}H- and ^{13}C- nuclear magnetic resonance (NMR) spectra were recorded in D_2O and DMSO-d_8 by Bruker Avance 400 operated at 400 MHz and 100 MHz, respectively. Chemical shifts (δ) are reported in parts per million (ppm) relative to residual H_2O (δ = 4.78 ppm) and DMSO peaks (δ = 2.46 ppm and 39.8 ppm for ^{1}H- and ^{13}C-NMR spectroscopy, respectively). Mass spectra were obtained by the HR-MALDI-TOF-MS. The absorption spectra were measured using an Agilent Cary 60 UV-vis spectrophotometer at room temperature, and the ATR-FTIR spectra were recorded using a Bruker Vertex 80-ATR. The CFP (avcarb-gds3250) was obtained from Fuel Cell Store in the United States, and the ITO-glass was purchased from Semiconductor Wafer, Inc. The Sustainion® X37-50 Grade RT AEM was supplied by Dioxide Materials, and PTFE 60 wt% dispersion in water and the Pt wire with a purity of 99.99% was obtained from Sigma Aldrich. The flow rate of 99.995% pure CO_2 gas was controlled using a KOFLOC mass flow meter (model 3810DS II Series). The electrochemical data was recorded using a PGSTAT101, Metrohm AG and an VersaSTAT 3, AMETEK, Inc. The reduction products in the gas phase were determined using an Agilent 8890 GC system equipped with a thermal conductivity detector (TCD) and a select permanent gasses column (CP7429, Agilent), including set of two parallel columns of CP-Molsieve 5 Å for permanent gases analysis and CP-PoraBOND Q for CO_2 analysis.[32] Ultra-high purity He gas was used as a carrier gas for the detection of N_2, O_2, CO_2, H_2, CH_4, C_2H_4, and CO, and standard gases were used for calibration. The flow rate of the electrolyte solution was controlled using a LEADFLUID Peristaltic Pump (BT100 S).

Synthesis of 4,9,16,23-Tetraaminophthalocyaninatonickel(II) (NiTAPc)

Following a published protocol[21] with slight modification with a type of starting material and a purification step, a mixture of 4-nitrophthalonitrile (**1**, 0.865, 5.00 mmol), nickel acetate tetrahydrate (0.323 g, 1.30 mmol), urea (0.15 g, 25 mmol), and ammonium molybdate tetrahydrate (0.026 g, 0.0050 mmol) was stirred in nitrobenzene at 185 °C for 4 hours. After cooling to room temperature, the reaction mixture was poured into methanol and filtered. The resulting precipitate was then washed repeatedly with methanol, dichloromethane, and hexanes to yield a dark green solid containing 4,9,16,23-tetranitrophthalocyaninato-nickel(II), which was subjected to a reduction step without any further treatment. A solution of this solid (0.806 g, 1.07 mmol) and $NaS \cdot 9H_2O$ (3.2 g, 13 mmol) in DMF (5.0 mL) was heated at 60 °C for 2 hours under N_2 atmosphere. After that the reaction mixture was cooled to room temperature and poured into iced water. The resulting precipitate was collected and washed with methanol using centrifugation. After the removal of a liquid phase, the solid was dried under ambient atmosphere, ground into fine powder, and washed with dichloromethane and hexanes using centrifugation to remove remaining impurity. The compound was then dried to afford a dark green solid (0.443 g, 56% from compound **1**). HR-MALDI-TOF MS (m/z): $[M]^+$ calcd for $C_{32}H_{20}N_{12}Ni$, 630.1287; found 630.1291.

Synthesis of 4,9,16,23-Tetraaminophthalocyaninatocobalt(II) (CoTAPc)

Following a procedure described for **NiTAPc** by using cobalt acetate tetrahydrate (0.323 g, 1.30 mmol), the title compound was obtained as a dark green solid (0.395 g, 50% from compound **1**). HR-MALDI-TOF MS (m/z): $[M]^+$ calcd for $C_{32}H_{20}N_{12}Co$, 631.1266; found 631.1291.

Preparation of the MPL-CFP Substrate

The commercial CFP was cut to a size of 2.5 cm×2.5 cm and preheated to 300 °C. On a side having the water repelling MPL, an area of 1 cm×1 cm was covered with the Ti plate of the same size to create an area for the electropolymerization of the monomers. To prevent the electropolymerization and to create an insulating hydrophobic layer on the remaining area, including the other side of the substrate, a layer of PTFE was coated by hand-spray coating (airbrush) using a 10 wt% PTFE dispersion in water. After each spraying, the substrate was left to dry on a hot plate before the next spraying was repeated for additional 9 times. After that, the resulting substrated was left to dry at 300 °C for 30 minutes, resulting in the PTFE-CFP. Subsequently, the Ti plate was removed from the MPL side to obtain a 1 cm×1 cm MPL-CFP substrate ready for the electropolymerization.

Electropolymerization of NiTAPc and CoTAPc

The electropolymerization was performed on the ITO-glass and the above-mentioned 1 cm×1 cm MPL-CFP substrate to obtain the films for the film characterization and for the catalytic performance studies, respectively. The ITO-glass was cut to a size of 0.8 cm×4.0 cm and wiped with toluene soaked KimWipes paper. After that, the resulting ITO-glass substrate was washed with acetone, isopropanol and deionized water under sonication for 15 minutes, and then dried in an oven at 100 °C for 15 minutes. The MPL-CFP substrate was washed with acetone and then dried in the oven at 100 °C for 15 minutes. The electropolymerization of **NiTAPc** or **CoTAPc** was conducted by means of the CV in a one-compartment three-electrode system having the ITO-glass or MPL-CFP as the WE, the Pt wire as the CE, and the Ag/AgCl QRE equipped with a porous glass frit junction. The Ag/AgCl QRE was calibrated using a ferrocenium/ferrocene (Fc^+/Fc) redox couple in a 0.1 M $TBAPF_6$ solution in DMF as an external standard. The potentials were converted to an NHE scale using the standard potential (E°) of Fc^+/Fc = 0.72 V *vs.* NHE in DMF.[16a] The 0.1 M $TBAPF_6$ in DMAc was used as the supporting electrolyte and contained 0.5 mM **NiTAPc** or **CoTAPc**. Prior to each experiment, N_2 was purged through the electrolyte solution at a flow rate of 50 $mL \cdot min^{-1}$ for 15 minutes. The electropolymerization was carried out by applying the potential between of −0.33 V to 1.27 V *vs.* NHE at the scan rate of 50 $mV \cdot s^{-1}$ for 10 and 20 cycles to cover the area of 0.8 cm×2.0 cm and 1 cm×1 cm of the ITO-glass and the MPL-CFP, respectively, with **p-**

© 2024 Wiley-VCH GmbH

NiTAPc. In the case of the electropolymerization of **CoTAPc**, the number of the scanning cycle was increased to 20 and 40 to obtain sufficient coverage of **p-CoTAPc** on the the ITO-glass and the MPL-CFP, respectively. After the electropolymerization process was completed, the resulting films were washed with DMAc to eliminate the remaining monomer and electrolyte, dried on the hot plate at 100 °C for 1 hour and then left under reduced pressure in a vacuum desiccator overnight.

Catalytic Performance Studies on the CO_2RR

The flow cell consisted of 3 PTFE plates stacked and held together by the silicone rubber sheets, stainless steel bolts and nuts.[33] Each plate was patterned by using a CNC milling machine to create a serpentine-shape gas flow channel, and the catholyte and anolyte chambers. The WE was the 1 cm×1 cm **p-NiTAPc**/MPL-CFP or **p-CoTAPc**/MPL-CFP connected with the Ti plate current collector and placed in the catholyte chamber. The anolyte one contained the Pt wire, serving as the CE, that was attached with another titanium plate current collector, and the commercial Ag/AgCl (3 M KCl) RE that was calibrated with the Fc^+/Fc redox couple in a 1 M KCl aqueous solution. The Sustainion® X37-50 Grade RT was used as the AEM and placed between the catholye and anolyte chambers. The flow rate of CO_2 gas was controlled by the KOFLOC mass flow meter at 10 mL·min^{-1}. The electrolyte was pumped through silicone tubes at the flow rate of 15 mL·min^{-1}, and flown between the flow cell electrolyzer and a 200-mL electrolyte reservoir of each chamber. During the CPE experiment at the current densities of $>$10 mA, the potentials were adjusted with iR-compensation at 80% using positive feedback through VersaStudio software. The potentials were then converted to an RHE scale using the equation RHE = E *vs.* Ag/AgCl (3 M KCl) + 0.059(pH) + 0.21 V − iRu, where i and Ru represent an average current value and an uncompensated solution resistance, respectively. For the **p-NiTAPc**/MPL-CFP and **p-CoTAPc**/MPL-CFP in the flow cell using the 1 M $KHCO_3$ aqueous solution, the resistance of approximately 7–8 ohms was detected and corrected before conducting each experiment.

Quantitative Determination of the Reduction Products

A gas mixture from the gas outlet of the flow cell was analyzed using the Agilent Technologies 8890 GC system, which was equipped with the TCD and two parallel columns (CP-Molsieve 5 Å and CP-PoraBOND Q). These columns separated and quantified the gas mixture, including H_2, O_2, N_2, CO, and CO_2, in a single run. The amounts of all the separated gases were calibrated using mixtures of each standard gas with N_2. The GC system was operated at 150 °C for the TCD detector and 35 °C for the oven during the separation of the gas products for 6 minutes. An oven temperature was then increased to 200 °C for column cleaning at a ramp rate of 120 °C·min^{-1} for 5 minutes. The ultra-high purity He gas was used as the carrier gas and introduced into the column at a ramped pressure of 8 psi for 3 minutes, followed by 25 psi for 8 minutes at the ramp rate of 100 psi·min^{-1}. An automatic sample loop was set to an equilibrium time of 3.75 minutes after cooling down, and then injected into the next round. This sequence condition allowed for the analysis of the reduction gas product(s) every 20 minutes during the CPE experiments. The flow rate of the gas mixture was controlled by the flow rate of CO_2 at the inlet, which was set at 10 mL·min^{-1} using the mass flow meter. The NMR spectroscopy was used to investigate the products in liquid phases in D_2O and DMSO-d_8. The results indicated that there was no carbon-based reduction product in any samples.

Supporting Information

Characterization data of the target monomers, cyclic voltammetric data of the target polymers and microscopic images of the electrode samples, as well as performance comparison table.

Acknowledgements

This research was partially supported by funding for high-efficiency postdoc researchers under the Second Century Fund (C2F) and Thailand Science research and Innovation Fund Chulalongkorn University. Talent mobility was supported by The Program Management Unit for Human Resources & Institutional Development, Research and Innovation (B16F640166). We also gratefully acknowledge the partial financial support of the Austrian Foundation for Advancement of Science (FWF Z222-N19) within the Wittgensteinprize for Prof. Sariciftci. Moreover, the authors would like to thank Dr. Jacek Gasiorowki for his heartfelt support as a great colleague and forever friend.

Conflict of Interests

The authors declare no conflict of interest.

Data Availability Statement

The data that support the findings of this study are available on request from the corresponding author. The data are not publicly available due to privacy or ethical restrictions.

Keywords: Cobalt(II)-phthalocyanine · Nickel(II)-phthalocyanine · Carbon dioxide conversion · Electrochemical carbon dioxide reduction · CCUS

[1] a) R. K. Pachauri, M. R. Allen, V. R. Barros, J. Broome, W. Cramer, R. Christ, J. A. Church, L. Clarke, Q. Dahe, P. Dasgupta, *Climate change 2014: synthesis report. Contribution of Working Groups I, II and III to the fifth assessment report of the Intergovernmental Panel on Climate Change*, Ipcc, **2014**; b) H.-O. Pörtner, D. C. Roberts, H. Adams, C. Adler, P. Aldunce, E. Ali, R. A. Begum, R. Betts, R. B. Kerr, R. Biesbroek, *Climate change 2022: Impacts, adaptation and vulnerability*, IPCC Geneva, Switzerland, **2022**.
[2] E. Alper, O. Yuksel Orhan, *Petroleum* **2017**, *3*, 109–126.
[3] a) B. Hu, C. Guild, S. L. Suib, *J. CO2 Util.* **2013**, *1*, 18–27; b) A. D. Tjandra, J. Huang, *Chin. Chem. Lett.* **2018**, *29*, 734–746.
[4] a) K. P. Kuhl, T. Hatsukade, E. R. Cave, D. N. Abram, J. Kibsgaard, T. F. Jaramillo, *J. Am. Chem. Soc.* **2014**, *136*, 14107–14113; b) F.-Y. Gao, R.-C. Bao, M.-R. Gao, S.-H. Yu, *J. Mater. Chem. A* **2020**, *8*, 15458–15478.
[5] a) X. Fang, S. Kalathil, E. Reisner, *Chem. Soc. Rev.* **2020**, *49*, 4926–4952; b) E. Daneshvar, R. J. Wicker, P.-L. Show, A. Bhatnagar, *Chem. Eng. J.* **2022**, *427*, 130884.
[6] L. Ai, S.-F. Ng, W.-J. Ong, *Environ. Chem. Lett.* **2022**, *20*, 3555–3612.
[7] Y. Pei, H. Zhong, F. Jin, *Energy Sci. Eng.* **2021**, *9*, 1012–1032.
[8] Y. Hori, H. Wakebe, T. Tsukamoto, O. Koga, *Electrochim. Acta* **1994**, *39*, 1833–1839.
[9] J. He, N. J. J. Johnson, A. Huang, C. P. Berlinguette, *ChemSusChem* **2018**, *11*, 48–57.

© 2024 Wiley-VCH GmbH

18673899, 0, Downloaded from https://chemistry-europe.onlinelibrary.wiley.com/doi/10.1002/cctc.202400281 by Faculty Of Medicine, Library Chulalongkorn University, Wiley Online Library on [09/06/2024]. See the Terms and Conditions (https://onlinelibrary.wiley.com/terms-and-conditions) on Wiley Online Library for rules of use; OA articles are governed by the applicable Creative Commons License

[10] a) S. Huo, Z. Weng, Z. Wu, Y. Zhong, Y. Wu, J. Fang, H. Wang, *ACS Appl. Mater. Interfaces* **2017**, *9*, 28519–28526; b) E. Tayyebi, J. Hussain, Y. Abghoui, E. Skúlason, *J. Phys. Chem. C* **2018**, *122*, 10078–10087.
[11] M. Asadi, K. Kim, C. Liu, A. V. Addepalli, P. Abbasi, P. Yasaei, P. Phillips, A. Behranginia, J. M. Cerrato, R. Haasch, P. Zapol, B. Kumar, R. F. Klie, J. Abiade, L. A. Curtiss, A. Salehi-Khojin, *Science* **2016**, *353*, 467–470.
[12] a) J. H. Zagal, F. Bedioui, J.-P. Dodelet, *N4-macrocyclic metal complexes*, Springer Science & Business Media, **2007**; b) F. Franco, C. Rettenmaier, H. S. Jeon, B. Roldan Cuenya, *Chem. Soc. Rev.* **2020**, *49*, 6884–6946; c) J.-W. DuanMu, Z.-Z. Wu, F.-Y. Gao, P.-P. Yang, Z.-Z. Niu, Y.-C. Z., L.-P. Chi, M.-R. Gao, *Precis.Chem.* **2024**, *2*, 151–160.
[13] a) Y. Wu, Y. Liang, H. Wang, *Acc. Chem. Res.* **2021**, *54*, 3149–3159; b) Q. Chang, Y. Liu, J.-H. Lee, D. Ologunagba, S. Hwang, Z. Xie, S. Kattel, J. H. Lee, J. G. Chen, *J. Am. Chem. Soc.* **2022**, *144*, 16131–16138.
[14] M. Li, C. Yan, R. Ramachandran, Y. Lan, H. Dai, H. Shan, X. Meng, D. Cui, F. Wang, Z.-X. Xu, *Chem. Eng. J.* **2022**, *430*, 133050.
[15] a) Z. Jiang, Y. Wang, X. Zhang, H. Zheng, X. Wang, Y. Liang, *Nano Res.* **2019**, *12*, 2330–2334; b) J. Choi, P. Wagner, S. Gambhir, R. Jalili, D. R. MacFarlane, G. G. Wallace, D. L. Officer, *ACS Energy Lett.* **2019**, *4*, 666–672.
[16] a) J. Luangchaiyaporn, D. Wielend, D. Solonenko, H. Seelajaroen, J. Gasiorowski, M. Monecke, G. Salvan, D. R. T. Zahn, N. S. Sariciftci, P. Thamyongkit, *Electrochim. Acta* **2021**, *367*, 137506; b) M. Krzywiecki, S. Pluczyk-Małek, P. Powroźnik, C. Ślusarczyk, W. Król-Molenda, S. Smykała, J. Kurek, P. Koptoń, M. Łapkowski, A. Blacha-Grzechnik, *J. Phys. Chem. C* **2021**, *125*, 13542–13550.
[17] a) H. Liu, J. Chu, Z. Yin, X. Cai, L. Zhuang, H. Deng, *Chem* **2018**, *4*, 1696–1709; b) A. M. Varghese, G. N. Karanikolos, *Int. J. Greenhouse Gas Control* **2020**, *96*, 103005.
[18] a) K. S. Lokesh, A. Adriaens, *Dyes Pigm.* **2015**, *112*, 192–200; b) N. Manjunatha, M. Imadadulla, K. R. V. S Lokesh, Reddy, *Dyes Pigm.* **2018**, *153*, 213–224.
[19] a) D. M. Weekes, D. A. Salvatore, A. Reyes, A. Huang, C. P. Berlinguette, *Acc. Chem. Res.* **2018**, *51*, 910–918; b) R. A. Tufa, D. Chanda, M. Ma, D. Aili, T. B. Demissie, J. Vaes, Q. Li, S. Liu, D. Pant, *Appl. Energy* **2020**, *277*, 115557; c) Y. Yang, F. Li, *Curr. Opin. Green Sustain. Chem.* **2021**, *27*; d) H. Wu, M. Zeng, X. Zhu, C. Tian, B. Mei, Y. Song, X.-L. Du, Z. Jiang, L. He, C. Xia, S. Dai, *ChemElectroChem* **2018**, *5*, 2717–2721.
[20] a) R. Shi, J. Guo, X. Zhang, G. I. N. Waterhouse, Z. Han, Y. Zhao, L. Shang, C. Zhou, L. Jiang, T. Zhang, *Nat. Commun.* **2020**, *11*, 3028; b) W. Luo, J. Zhang, M. Li, A. Züttel, *ACS Catal.* **2019**, *9*, 3783–3791.
[21] J. Alzeer, P. J. C. Roth, N. W. Luedtke, *Chem. Commun.* **2009**, 1970–1971.
[22] a) H. Li, T. F. Guarr, *J. Chem. Soc. Chem. Commun.* **1989**, 832–834; b) A. Goux, F. Bedioui, L. Robbiola, M. Pontié, *Electroanalysis* **2003**, *15*, 969–974; c) M. L'Her, A. Pondaven, in *The Porphyrin Handbook* (Eds.: K. M. Kadish, K. M. Smith, R. Guilard), Academic Press, Amsterdam, **2003**, pp. 117–169; d) M. Isaacs, F. Armijo, G. Ramírez, E. Trollund, S. R. Biaggio, J. Costamagna, M. J. Aguirre, *J. Mol. Catal. A* **2005**, *229*, 249–257; e) A. Sivanesan, S. A. John, *Electrochim. Acta* **2008**, *53*, 6629–6635.
[23] J. Pavez, M. Páez, A. Ringuedé, F. Bedioui, J. H. Zagal, *J. Solid State Electrochem.* **2005**, *9*, 21–29.
[24] a) A. W. Snow, in *The Porphyrin Handbook* (Eds.: K. M. Kadish, K. M. Smith, R. Guilard), Academic Press, Amsterdam, **2003**, pp. 129–176; b) X.-F. Zhang, Q. Xi, J. Zhao, *J. Mater. Chem.* **2010**, *20*, 6726–6733.
[25] C. Solis, E. Baigorria, M. E. Milanesio, G. Morales, E. N. Durantini, L. Otero, M. Gervaldo, *Electrochim. Acta* **2016**, *213*, 594–605.
[26] M. Trchová, J. Stejskal, *Pure Appl. Chem.* **2011**, *83*, 1803–1817.
[27] a) D. Zhang, *Polym. Test.* **2007**, *26*, 9–13; b) I. Šeděnková, J. Prokeš, M. Trchová, J. Stejskal, *Polym. Degrad. Stab.* **2008**, *93*, 428–435; c) M. Ilic, E. Koglin, A. Pohlmeier, H. D. Narres, M. J. Schwuger, *Langmuir* **2000**, *16*, 8946–8951.
[28] P. J. Larkin, in *Infrared and Raman Spectroscopy (Second Edition)* (Ed.: P. J. Larkin), Elsevier, **2018**, pp. 85–134.
[29] a) X. Zhang, Y. Wang, M. Gu, M. Wang, Z. Zhang, W. Pan, Z. Jiang, H. Zheng, M. Lucero, H. Wang, G. E. Sterbinsky, Q. Ma, Y.-G. Wang, Z. Feng, J. Li, H. Dai, Y. Liang, *Nat. Energy* **2020**, *5*, 684–692; b) K. Chen, M. Cao, Y. Lin, J. Fu, H. Liao, Y. Zhou, H. Li, X. Qiu, J. Hu, X. Zheng, M. Shakouri, Q. Xiao, Y. Hu, J. Li, J. Liu, E. Cortés, M. Liu, *Adv. Funct. Mater.* **2022**, *32*, 2111322.
[30] N. Han, Y. Wang, L. Ma, J. Wen, J. Li, H. Zheng, K. Nie, X. Wang, F. Zhao, Y. Li, J. Fan, J. Zhong, T. Wu, D. J. Miller, J. Lu, S.-T. Lee, Y. Li, *Chem* **2017**, *3*, 652–664.
[31] a) M. E. Leonard, L. E. Clarke, A. Forner-Cuenca, S. M. Brown, F. R. Brushett, *ChemSusChem* **2020**, *13*, 400–411; b) K. Yang, R. Kas, W. A. Smith, T. Burdyny, *ACS Energy Lett.* **2021**, *6*, 33–40; c) J. Chen, L. Wang, *Adv. Mater.* **2022**, *34*, 2103900; d) W. Lai, Y. Qiao, Y. Wang, H. Huang, *Adv. Mater.* **2023**, *35*, 2306288.
[32] Agilent Technologies, "Select Permanent Gases Columns", can be found under https://www.agilent.com/en/product/gc-columns/application-specific-gc-columns/select-permanent-gasses-columns, **2024**.
[33] K. Liu, W. A. Smith, T. Burdyny, *ACS Energy Lett.* **2019**, *4*, 639–643.

Manuscript received: February 8, 2024
Revised manuscript received: April 27, 2024
Accepted manuscript online: May 2, 2024
Version of record online: ■■, ■■

© 2024 Wiley-VCH GmbH

18673899, 0, Downloaded from https://chemistry-europe.onlinelibrary.wiley.com/doi/10.1002/cctc.202400281 by Faculty Of Medicine, Library Chulalongkorn University, Wiley Online Library on [09/06/2024]. See the Terms and Conditions (https://onlinelibrary.wiley.com/terms-and-conditions) on Wiley Online Library for rules of use; OA articles are governed by the applicable Creative Commons License

RESEARCH ARTICLE

Hightly efficient electrocatalysts were prepared via facile electropolymerization of Ni^{II}- and Co^{II}-tetraaminophthalocyanines. Under optimized heterogeneous electrochemical CO_2 reduction condition in a customized flow cell, the target polymer films exhibited excellent catalytic performance for CO_2-to-CO conversion in terms of stability, productivity and selectivity. This study demonstrated a promising approach for development of scalable and practical electrochemial CO_2 reduction process.

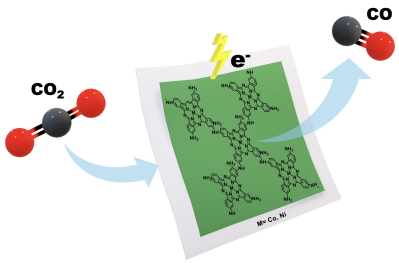

*Dr. J. Luangchaiyaporn, P. Chairat, R. Sodkhomkhum, Prof. Mag. Dr. DDr. N. S. Sariciftci, Prof. Dr. P. Thamyongkit**

1 – 11

Facile Preparation of Stable Ni^{II}- and Co^{II}-Tetraaminophthalocyanine Electropolymers for Highly Efficient Heterogeneous Carbon Dioxide Reduction

18673899, 0, Downloaded from https://chemistry-europe.onlinelibrary.wiley.com/doi/10.1002/cctc.202400281 by Faculty Of Medicine, Library Chulalongkorn University, Wiley Online Library on [09/06/2024]. See the Terms and Conditions (https://onlinelibrary.wiley.com/terms-and-conditions) on Wiley Online Library for rules of use; OA articles are governed by the applicable Creative Commons License